4. Palomares, F., Gaona, P., Ferreras, P. & Delibes, M. Positive effects on game species of top predators by controlling smaller predator populations: an example with lynx, mongooses, and rabbits. *Conserv. Biol.* **9,** 295–305 (1995).
5. Rogers, C. M. & Caro, M. J. Song sparrows, top carnivores, and nest predation: a test of the mesopredator release hypothesis. *Oecologia* **116,** 227–233 (1998).
6. Soulé, M. E. & Terborgh, J. *Continental Conservation: Scientific Foundations for Regional Reserve Networks* (Island, Washington, 1999).
7. Estes, J. A. in *Linking Species and Ecosystems* (eds Jones, C. G. & Lawton, L. H.) 151–158 (Chapman and Hall, New York, 1995).
8. Litvaitis, J. A. & Villafuerte, R. Intraguild predation, mesopredator release, and prey stability. *Conserv. Biol.* **10,** 676–677 (1996).
9. Wright, S. J., Gompper, M. E. & Deleon, B. Are large predators keystone species in neotropical forests—the evidence from Barro-Colorado Island. *Oikos* **71,** 279–294 (1994).
10. Wilcove, D. S. Nest predation in forest tracts and the decline of migratory songbirds. *Ecology* **66,** 1211–1214 (1985).
11. Churcher, J. B. & Lawton, J. H. Predation by domestic cats in an English village. *J. Zool. (Lond.)* **212,** 439–456 (1987).
12. Leimgruber, P., McShea, W. J. & Rappole, J. H. Predation on artificial nests in large forest blocks. *J. Wildl. Mgmt* **58,** 254–260 (1994).
13. Fretwell, S. D. Food chain dynamics: the central theory of ecology? *Oikos* **50,** 291–301 (1987).
14. George, W. Domestic cats as predators and factors in winter shortages of raptor prey. *Wilson Bull.* **86,** 384–396 (1974).
15. Bolger, D. T., Alberts, A. & Soulé, M. E. Occurrence patterns of bird species in habitat fragments: sampling, extinction, and nested species subsets. *Am. Nat.* **137,** 155–166 (1991).
16. Linhart, S. B. & Knowlton, F. F. Determining the relative abundance of coyotes by scent station lines. *Wildl. Soc. Bull.* **3,** 119–124 (1975).
17. Conner, M. C., Labisky, R. F. & Progulske, D. R. Jr Scent-station indices as measures of population abundance for bobcats, raccoons, gray foxes, and opossums. *Wildl. Soc. Bull.* **11,** 146–152 (1983).
18. Bendel, R. B. & Afifi, A. A. Comparison of stepping rules in forward regression. *J. Am. Stat. Assoc.* **72,** 46–53 (1977).
19. Tabachnick, B. G. & Fidell, L. S. *Using Multivariate Statistics* 3rd edn (HarperCollins College Publishers, New York, 1996).

Acknowledgements. We thank L. Angeloni, D. Bolger, T. Case, J. Crooks, D. Doak, J. Estes, R. Fisher, S. Hathaway, D. Menendez, S. Minta, P. Raimondi, B. Rice, and A. Suarez for their valuable help with this research, and C. Bell for illustrating Fig. 1. This work was funded by D. Brimm, an NSF Graduate Research Fellowship, an EPA STAR Fellowship and an American Society of Mammalogist grant (K.R.C.).

Correspondence and requests for materials should be addressed to K.R.C. (e-mail: krcrooks@earthlink.net.).

Linking a genetic defect to its cellular phenotype in a cardiac arrhythmia

Colleen E. Clancy* & Yoram Rudy*†

*Cardiac Bioelectricity Research and Training Center, † Department of Biomedical Engineering and * Department of Physiology and Biophysics, Case Western Reserve University, Cleveland, Ohio 44106-7207, USA*

Advances in genetics and molecular biology have provided an extensive body of information on the structure and function of the elementary building blocks of living systems. Genetic defects in membrane ion channels can disrupt the delicate balance of dynamic interactions between the ion channels and the cellular environment, leading to altered cell function[1–3]. As ion-channel defects are typically studied in isolated expression systems, away from the cellular environment where they function physiologically, a connection between molecular findings and the physiology and pathophysiology of the cell is rarely established. Here we describe a single-channel-based Markovian modelling approach that bridges this gap. We achieve this by determining the cellular arrhythmogenic consequences of a mutation in the cardiac sodium channel that can lead to a clinical arrhythmogenic disorder (the long-QT syndrome) and sudden cardiac death.

Several distinct genetic mutations in the *SCN5A* gene give rise to a congenital form of the long-QT syndrome and have been mapped to the α-subunit of the cardiac sodium channel (LQT3)[4]. The most severe is the ΔKPQ mutation, a three-amino-acid deletion of Lys 1505, Pro 1506 and Gln 1507 in the highly conserved portion of the III–IV linker, which is responsible for fast inactivation[5]. Clinically, the ΔKPQ mutation is associated with substantial prolongation of the Q–T interval on the electrocardiogram, which may precede syncope and sudden cardiac death.

To evaluate the electrophysiological consequences of the ΔKPQ defect at the level of the cardiac action potential, we constructed Markov models of the wild-type and ΔKPQ mutant channels based on experimental data[5–7]. The models were then integrated into the Luo–Rudy theoretical model of the cardiac ventricular action potential[8–10].

The Markovian models for the wild-type and ΔKPQ sodium channel are shown in Fig. 1. The wild-type channel model (Fig. 1a) includes three closed states (C3, C2 and C1), a conducting open state (O), and fast and slow inactivation states (IF and IS, respectively). The mutant channel model (Fig. 1b) contains two possible modes of gating, a 'background (dispersed) mode' and a 'burst mode'. The background mode includes the above six states (Fig. 1b); it is similar to the wild-type model except for alterations in the voltage dependence of activation, inactivation and recovery from inactivation (Box 1). Most (>99%) of the mutant channels reside in the background mode states. The models were incorporated into the Luo–Rudy model (Fig. 1c) for action potential simulations.

Box 1 Simulation methods

The general approach to modelling the action potential is the same as that described for the Luo–Rudy model[8–10] except that the I_{Na} transmembrane current is reformulated from the single-channel kinetics. We use the general approach of refs 20 and 21. All kinetic parameters were normalized to 37 °C with a Q_{10} of 3 (ref. 19).

All the simulations were encoded in C/C^{++}. Simulations were implemented (double precision) on a Sun Workstation Ultra 1. A time step of 0.005 ms was used during the stimulus and the action potential upstroke. At all other times, a 0.01-ms time step was used.

Transition rates

Wild-type channel (ms^{-1});

C3 → C2 $\alpha 11 = 3.802/(0.1027 \times \exp(-v/17.0) + 0.20 \times \exp(v/150))$
C2 → C1 $\alpha 12 = (3.802/(0.1027 \times \exp(-v/15.0) + 0.23 \times \exp(-v/150)))$
C1 → O $\alpha 13 = 3.802/(0.1027 \times \exp(-v/12.0) + 0.250 \times \exp(-v/150))$
C2 → C3 $\beta 11 = 0.1917 \times \exp(-v/20.3)$
C1 → C2 $\beta 12 = 0.20 \times \exp(-(v-5)/20.3)$
O → C1 $\beta 13 = 0.22 \times \exp(-(v-10)/20.3)$
O → IF $\alpha 2 = (9.178 \times \exp(v/29.68))$
IF → O $\beta 2 = ((\alpha 13 \times \alpha 2 \times \alpha 3)/(\beta 13 \times \beta 3))$
IF → C1 $\alpha 3 = (3.7933^{-9} \times \exp(-v/5.2))$
C1 → IF $\beta 3 = (0.0084 + 0.00002 \times v)$
IF → IS $\alpha 4 = \alpha 2/100$
IS → IF $\beta 4 = \alpha 3$

ΔKPQ mutant channel* (ms^{-1}):

xC3 → xC2
$\alpha 11 = 1.25 \times (3.082/(0.1027 \times \exp(-v/17.0) + 0.20 \times \exp(-v/150)))$
xC2 → xC1
$\alpha 12 = 1.25 \times (3.082/(0.1027 \times \exp(-v/15.0) + 0.23 \times \exp(-v/150)))$
xC1 → xO
$\alpha 13 = 1.25 \times (3.082/(0.1027 \times \exp(-v/12.0) + 0.250 \times \exp(-v/150)))$
xC2 → xC3 $\beta 11 = 0.1917 \times \exp(-v/20.3)$
xC1 → xC2 $\beta 12 = 0.20 \times \exp(-(v-5)/20.3)$
xO → xC1 $\beta 13 = 0.22 \times \exp(-(v-10)/20.3)$
O → IF $\alpha 2 = (9.178 \times \exp(v/100))$
IF → O $\beta 2 = ((\alpha 13 \times \alpha 2 \times \alpha 3)/(\beta 13 \times \beta 3))$
IF → UC1 $\alpha 3 = 20 \times (3.7933^{-9} \times \exp(-v/5.2))$
UC1 → IF $\beta 3 = 2 \times (0.0084 + 0.00002 \times v)$
IF → IS $\alpha 4 = \alpha 2/100$
IS → IF $\beta 4 = \alpha 3$

* x represents U or L, as transition rates in the background or burst modes are the same.
Transition rates between modes are background to burst, $\mu 1 = 2 \times 10^{-6}$ ms^{-1}; burst to background, $\mu 2 = 1 \times 10^{-4}$ ms^{-1}.

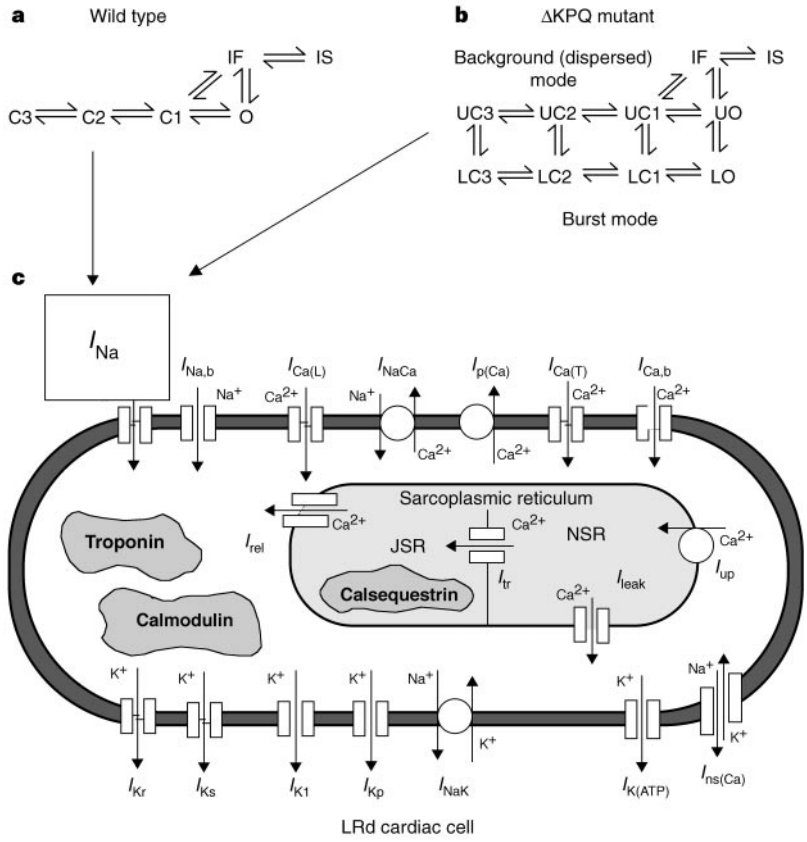

Figure 1 Markovian models of sodium channels. **a**, Wild-type (WT); **b**, ΔKPQ mutant. **c**, The Luo–Rudy dynamic cardiac-cell model (LRd)[8–10]. JSR, junctional sarcoplasmic reticulum; NSR, network sarcoplasmic reticulum.

Figure 2a shows simulated and experimentally measured[6] single-channel recordings. Like wild-type channels (Fig. 2a, WT), mutant channels in the background mode open and inactivate in response to depolarization (Fig. 2a, ΔKPQ, top three traces). Mutant channels activate more quickly (increased rate constants of activation). As the open and the inactivated states are strongly coupled, the increased probability of being in the open state leads to increased probability of inactivation and faster decay of the mutant macroscopic current compared to the wild type[6,7]. Mutant channels also recover from inactivation more rapidly than wild-type channels[11]. As channel availability is increased, a background current results from channel reopenings at depolarized membrane potentials (late openings following the first opening in Fig. 2a, ΔKPQ; top three traces). Thus, an increased rate of recovery from inactivation in the background mode leads to dispersed channel re-openings and a late component of I_{Na}.

The burst mode of the ΔKPQ channel model (Fig. 1b) does not include the inactivated states IF and IS. Being in this mode of the mutant channel corresponds to transient failure of the channel to inactivate (Fig. 1b). The likelihood of entry into the lower states of the ΔKPQ burst mode is very low ($2 \times 10^{-6}\,ms^{-1}$) but once channels are in these states, return to the background mode is unlikely ($10^{-4}\,ms^{-1}$). This results in a small population of channels in the lower states that fail to inactivate. These channels bounce back and forth between closed available states and a single open state (LC1, LC2 and LC3; and LO, respectively) (Fig. 2a, ΔKPQ; bottom two traces). Note the frequent opening events ('bursting') of channels in this mode. Together with the dispersed re-openings of channels in the background mode, this behaviour can result in a significant late current that causes marked changes in the action potential.

The mean open time (MOT) of simulated and measured ΔKPQ mutant channels is shown in Fig. 2b, with background mode in the top panels and burst mode in the bottom panels. The experiments show relatively weak voltage dependence for the MOT of background openings, as compared to strong voltage dependence for the MOT of burst-type openings[6]. This behaviour is reflected in the similarity of the MOT distributions for depolarization to −50 mV or −20 mV in the background mode, in contrast to the widening of the distribution in the burst mode at −20 mV compared to −50 mV. In our simulations, the voltage dependence of the MOT is reproduced by simply removing inactivation from the background mode (that is, being in the burst mode of the mutant channel model). In the absence of inactivation, the voltage dependence of bursting is dominated by deactivation (Fig. 1b, transition from LO to LC3). As the membrane potential is progressively depolarized, the deactivation transition becomes slower and the mean open time increases ($1/\beta 13$). In contrast, the weak voltage dependence of the background mode MOT ($1/(\beta 13 + \alpha 2)$) in this voltage range is due to the co-dominance of deactivation (transition from UO to UC3) and inactivation (transition from UO to IF)[12]. Increased depolarization results in a decrease in the deactivation transition rate that is balanced by a concomitant increase in the inactivation rate. This results in little dependence of the MOT on voltage in this range.

The additive effects of background channel reopenings and a small subpopulation of bursting channels on the macroscopic current are shown in Fig. 3a. In the wild-type channels, depolarization to −20 mV from a holding potential of −140 mV results in a large macroscopic current (peak $> 300\,\mu A\,\mu F^{-1}$) that fully inactivates and returns to zero. In contrast, a model cell with a 100% ΔKPQ mutant-channel population is marked by a persistent component ($0.3\,\mu A\,\mu F^{-1}$) of current even after prolonged depolarization (200 ms). Experimental data are shown for comparison (right panels)[7].

Figure 3b shows the accelerated decay of the early component of macroscopic sodium current in the ΔKPQ mutant, as seen

experimentally[6,7]. The cell is depolarized to −40 mV from a holding potential of −140 mV (inset). The increase in the rate of current decay results largely from an increased rate of activation. Faster activation (increased probability in UO) leads to an increased probability of inactivation and corresponding current decay. We compare simulated data to experimental data from ref. 6.

So far, we have established the capability of the Markov sodium-channel model to correctly reproduce single-channel behaviour and macroscopic current properties. We next investigated the cellular arrhythmogenic consequences of the ΔKPQ mutation by integrating the channel models into the Luo–Rudy model of the cardiac ventricular cell[8–10] (Fig. 1).

Figure 4A and B shows the action potential and sodium current (I_{Na}) from the tenth beat of a simulated cell, paced at a cycle length of 400 ms. In Fig. 4A, the cell contains 100% wild-type channels; in Fig. 4B the channels are ΔKPQ mutants. The mutant-cell action potential (Fig. 4B) has an increased depolarization rate compared to the wild type (325.9 and 296.9 V s^{-1}, respectively), as well as marked prolongation of the action potential duration (APD; 62.3 ms increase). Inspection of the corresponding sodium current at high gain (Fig. 4B, bottom) reveals a persistent component of inward current (3 μA $μF^{-1}$) during the plateau of the action potential. The morphology of the simulated current (Fig. 4B) compares well with experimentally recorded I_{Na} during an action potential clamp (Fig. 4D)[13]. Although the amplitude of the persistent current is very small, only 1.0% of the peak I_{Na} (>300 μA $μF^{-1}$), it is sufficient to shift the delicate balance of currents that exists during the action potential plateau[8–10,14]. The additional inward current carried by sodium acts in opposition to repolarizing outward currents and prolongs the APD. Figure 4C shows the effect of decreasing the pacing rate (cycle length from 400 ms to 600 ms) in the ΔKPQ mutant cell. The tenth beat is shown and demonstrates an arrhythmogenic early after-depolarization (EAD) that develops from plateau potentials[9,14]. At the slower rate, repolarizing outward currents (in particular the slow delayed rectifier, I_{Ks}) deactivate more completely between beats[10,14]. The combination of the persistent depolarizing I_{Na} and the reduced repolarizing I_{Ks} causes marked APD prolongation, which gives time for the L-type calcium current, $I_{Ca(L)}$, to recover from inactivation and reactivate. The secondary reactivation of $I_{Ca(L)}$ (not shown) depolarizes the membrane and generates the EAD[14]. A small population of bursting ΔKPQ channels ($P(LO) < 0.005$), in combination with dispersed channel re-openings ($P(UO) < 0.001$), contributes to the persistent inward current.

Transcription of both mutant and wild-type SCN5A alleles is likely to occur, as affected individuals are typically heterozygous for LQT3. To investigate this possibility, we simulated paced cells containing different WT:ΔKPQ ratios of Na^+ channels. Figure 4E shows the effects of varying the stoichiometry of wild-type and ΔKPQ channel populations in the cell. Action potentials from a wild-type cell paced for five beats at a cycle length of 1,000 ms are shown in Fig. 4E, a. As the percentage of ΔKPQ channels is increased relative to wild type (Fig. 4E, b–c), the APD becomes progressively longer and EAD development is marked. Note (Fig. 4E, b) that the presence of 50% mutant channels is sufficient to cause EADs at this rate (cycle length, 1,000 ms).

The development of arrhythmogenic episodes in congenital LQT3 is correlated with bradycardia during sleep or relaxation[15]. Faster pacing rates result in adaptive shortening of the APD and an

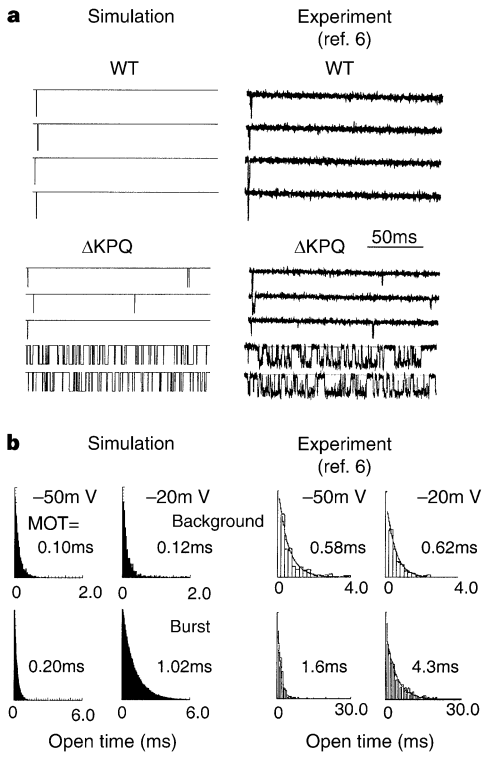

Figure 2 Single-channel properties of WT and mutant I_{Na}. **a**, Single-channel gating in simulated channels (left) and experimental recordings from ref. 6 (right). Top: wild-type (WT) channel gating. Bottom ΔKPQ mutant channel gating, where top three traces correspond to the mutant channel in the background mode and bottom two traces show burst opening in the burst mode. **b**, The MOT of ΔKPQ mutant channels. Simulations are compared to data from ref. 6. Differences in MOT are due to temperature differences and can be compensated for by a Q_{10} of 3 (ref. 19).

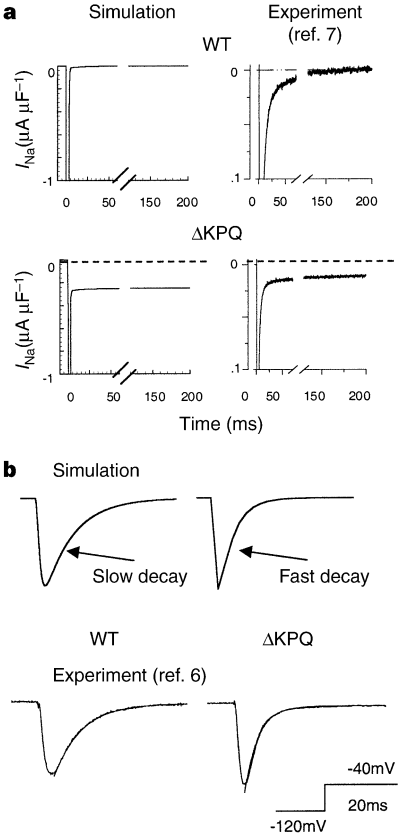

Figure 3 Macroscopic WT and mutant I_{Na}. **a**, Macroscopic I_{Na} during step depolarization from −140 to −20 mV. Top: Wild-type channels. I_{Na} inactivates and returns to zero. Bottom: ΔKPQ channels. There is a persistent component of I_{Na}. Simulations (left) are compared to normalized data from ref. 7 (right). **b**, Increased rate of macroscopic current decay in ΔKPQ mutant channels. Simulations (top) are compared to data from ref. 6 (bottom). Protocol is shown in inset.

accompanying shortening of the Q–T interval in the ECG. To investigate the cellular response to changes in cycle length, we chose a WT:ΔKPQ ratio of 50:50. Figure 4F shows the response of the cell to bradycardia, tachycardia and normal physiological cycle length. Figure 4F, a shows the fourth and fifth beats at rapid pacing (cycle length, 400 ms). Note the absence of EADs and adaptive shortening of the action potential duration at faster cycle length. At a normal human cycle length (Fig. 4F, b), the action potential duration is markedly prolonged relative to the wild type. When the cell is exposed to bradycardia (cycle length, 1,200 ms; Fig. 4F, c), hallmark EADs develop after several beats and are sustained during subsequent pacing.

This study describes the effects of a genetic defect (ΔKPQ mutation) on the cardiac ventricular action potential and demonstrates its arrhythmogenic consequences at the cellular level. We have formulated a Markovian based model that represents discrete structural states and their interactions. Although the traditional Hodgkin–Huxley[16] type of model is useful for a variety of modelling efforts, this framework is insufficient for incorporation of state-specific structural channel defects. Strong coupling between discrete structural states (a property not represented in the Hodgkin–Huxley scheme) is required, as a mutation affecting the structural integrity of a particular state will affect adjacent states[17,18]. The theoretical tool introduced here allows the integration of single channels (wild-type or mutant) into the whole cell, where their effects on cellular behaviour can be studied. As more idiopathic diseases are linked to congenital abnormalities, modelling strategies of this type can help to bridge the gap between genetic molecular defects and their phenotypic consequences. □

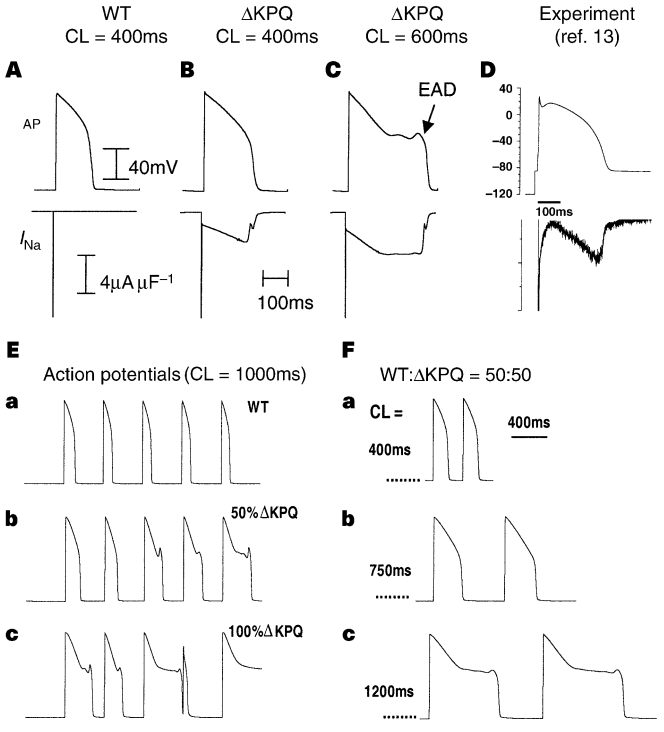

Figure 4 Effect of ΔKPQ mutation on the whole-cell action potential. **A**–**D**, Persistent I_{Na} during the action potential plateau (**B**) prolongs the action potential duration (compare to WT in **A**). Note close correspondence of the morphology of I_{Na} between simulation (**B**) and data from ref. 13 (**D**). Slowing the rate (**C**) results in further APD prolongation and EAD development. **E**, The effects of varying the WT:ΔKPQ channel stoichiometry within a single cell. The cell is paced at a cycle length of 1,000 ms for five beats. 50% mutant channels are sufficient to cause EADs. **F**, Effect of pacing cycle length on EAD development. Cells contain 50% mutant channel population and are paced for five beats at the indicated cycle length (CL) (4th and 5th beats are shown).

Received 23 March; accepted 8 June 1999.

1. Welsh, M. J. & Hoshi, T. Ion channels lose the rhythm. *Nature* **376,** 640 (1995).
2. Attali, B. A new wave for heart rhythms. *Nature* **384,** 24–25 (1996).
3. Keating, M. T. & Sanguinetti, M. C. Molecular genetic insights into cardiovascular disease. *Science* **272,** 681–685 (1996).
4. Barinaga, M. Tracking down mutations that can stop the heart. *Science* **281,** 32–34 (1998).
5. Dumaine, R. *et al.* Multiple-mechanisms of Na^+ channel-linked long-QT syndrome. *Circ. Res.* **78,** 916–924 (1996).
6. Chandra, R., Starmer, C. F. & Grant, A. O. Multiple effects of the KPQ deletion on gating of human cardiac Na^+ channels expressed in mammalian cells. *Am. J. Physiol.* **274,** H1643–H1654 (1998).
7. Bennett, P. B., Yazawa, K., Makita, N. & George, A. L. Jr Molecular mechanism for an inherited cardiac arrhythmia. *Nature* **376,** 683–685 (1995).
8. Luo, C. H. & Rudy, Y. A dynamic model of the cardiac ventricular action potential. I. Simulations of ionic currents and concentration changes. *Circ. Res.* **74,** 1071–1096 (1994).
9. Luo, C. H. & Rudy, Y. A dynamic model of the cardiac ventricular action potential. II. After-depolarizations, triggered activity, and potentiation. *Circ. Res.* **74,** 1097–1113 (1994).
10. Zeng, J., Laurita, K. R., Rosenbaum, D. S. & Rudy, Y. Two components of the delayed rectifier K^+ current in ventricular myocytes of the guinea pig type. Theoretical formulation and their role in repolarization. *Circ. Res.* **77,** 140–152 (1995).
11. Wamg. D. W., Yazawa, K., George, A. L. Jr & Bennett, P. B. Characterization of human cardiac Na^+ channel mutations in the congenital long QT syndrome. *Proc. Natl Acad. Sci. USA* **93,** 13200–13205 (1996).
12. Yue, D. T., Lawrence, J. H. & Marban, E. Two molecular transitions influence cardiac sodium channel gating. *Science* **244,** 349–352 (1989).
13. Wang, D. W., Yazawa, K., Makita, N., George, A. L. Jr & Bennett, P. B. Pharmacological targeting of long QT mutant sodium channels. *J. Clin. Invest.* **99,** 1714–1720 (1997).
14. Zeng, J. & Rudy, Y. Early afterdepolarizations in cardiac myocytes: mechanism and rate dependence. *Biophys. J.* **68,** 949–964 (1995).
15. Schwartz, P. J. *et al.* Long QT syndrome patients with mutations of the SCN5A and HERG genes have differential responses to Na^+ channel blockade and to increases in heart rate. Implications for gene-specific therapy. *Circulation* **92,** 3381–3386 (1995).
16. Hodgkin, A. L. & Huxley, A. F. A quantitative description of membrane current and its application to conduction and excitation in nerve. *J. Physiol.* **117,** 500–544 (1952).
17. Tomaselli, G. F. *et al.* A mutation in the pore of the sodium channel alters gating. *Biophys. J.* **68,** 1814–1827 (1995).
18. Mitsuiye, T. & Noma, A. Inactivation of the cardiac Na^+ channels in guinea-pig ventricular cells through the open state. *J. Physiol.* **485**, 581–594 (1995); erratum *J. Physiol. (Lond.)* **488**, 841 (1995).
19. Hanck, D. A. in *Cardiac Electrophysiology: From Cell to Bedside* (eds Zipes, W. & Jalife, J.) 65–74 (W. B. Saunders, Philadelphia, 1995).
20. Balser, J. R., Roden, D. M. & Bennett, P. B. Global parameter optimization for cardiac potassium channel gating models. *Biophys. J.* **57,** 433–444 (1990).
21. Zeng, J. in *Biomedical Engineering* (Case Western Reserve Univ., Cleveland, 1997).

Acknowledgements. We thank P. Bennett and A. Grant for providing us with original figures from their experimental publications. This work was supported by the NIH-National Heart, Lung and Blood Institute and The Whitaker Foundation.

Correspondence and requests for materials should be addressed to Y.R. (e-mail: yxr@po.cwru.edu).

Developmental and activity-dependent regulation of kainate receptors at thalamocortical synapses

Fleur L. Kidd & John T. R. Isaac

MRC Centre for Synaptic Plasticity, Department of Anatomy, University of Bristol, Bristol BS8 1TD, UK

Most of the fast excitatory synaptic transmission in the mammalian brain is mediated by ionotrophic glutamate receptors, of which there are three subtypes: AMPA (α-amino-3-hydroxyl-5-methyl-4-isoxazolepropionate), NMDA (*N*-methyl-D-aspartate) and kainate. Although kainate-receptor subunits (GluR5–7, KA1 and 2) are widely expressed in the mammalian central nervous system[1,2], little is known about their function. The development of pharmacological agents that distinguish between AMPA and kainate receptors has now allowed the functions of kainate receptors to be investigated[3,4]. The modulation of synaptic transmission by kainate receptors[5–7] and their synaptic activation[8–14] in a variety of brain regions have been reported. The expression of kainate receptor subunits is developmentally regulated[1,2] but their role in plasticity and development is unknown. Here we show that developing thalamocortical synapses express postsynaptic kainate receptors as well as AMPA receptors; however, the two receptor subtypes do not co-localize. During the critical period for experience-dependent plasticity, the kainate-receptor contribution to transmission decreases; a similar decrease occurs when long-term potentiation